Available online at www.sciencedirect.com
ScienceDirect
Chemical Physics 338 (2007) 90–105
Chemical Physics
www.elsevier.com/locate/chemphys

Stereomutation dynamics in hydrogen peroxide

Benjamin Fehrensen, David Luckhaus [1], Martin Quack *

ETH Zürich, Laboratorium für Physikalische Chemie, Wolfgang-Pauli-Str. 10, CH-8093 Zürich, Switzerland

Received 3 May 2007; accepted 5 June 2007
Available online 20 June 2007

Dedicated to Jörn Manz on the occasion of his 60th birthday.

Abstract

Hydrogen peroxide (H–O–O–H) is among the simplest prototype molecules showing a chiral equilibrium geometry with the possibility of fast quantum stereomutation in the low barrier limit. We report full dimensional quantum dynamical tunneling calculations on a semi-global fully six-dimensional empirically adjusted potential hypersurface for H_2O_2, which is realistically close to spectroscopic and thermochemical accuracy (B. Kuhn, T.R. Rizzo, D. Luckhaus, M. Quack, M.A. Suhm, J. Chem. Phys. 111 (1999) 2565). Solutions of the time independent Schrödinger equation lead to levels of well defined parity (but undefined chirality), which compare well with available spectroscopic results and provide numerous predictions. Solutions of the time dependent Schrödinger equation with initial conditions of well defined chirality for P and M enantiomers show the time dependent wavepacket motion and periodic change of chirality for time scales between picoseconds and hundreds of picoseconds. Complete six-dimensional dynamics and adiabatic separation of the torsional mode from the high-frequency modes leads to essentially identical results for the stereomutation dynamics in terms of the relevant time dependence. Mode selective inhibition and catalysis of stereomutation by exciting various vibrationally excited levels are reported and discussed in relation to the concept of quasiadiabatic above barrier tunneling. The transition to relaxation behaviour and racemisation is demonstrated with quasithermal wavepackets and analysed in terms of a simple statistical model. At 3000 K the racemisation relaxation time is calculated to be 30 fs. We also discuss the results in the context of recent results on hydrogen peroxide as a prototype system for parity violation in chiral molecules.

Keywords: Hydrogen peroxide; Stereomutation; Tunneling; Racemisation; Chirality; Quantum wavepackets dynamics

1. Introduction

Time dependent quantum wavepacket motion in relation to intramolecular dynamics has a long and rich history going back to the origins of quantum mechanics ([1–6] and references therein). Particularly after the discovery [7–9] and theoretical description [10–13] of isotope selective coherent infrared multiphoton excitation and laser chemistry of polyatomic molecules and subsequently also the advent of "Femtosecond Chemistry" [14,15] there has been much interest in what has been called in a variety of contexts either "mode selective chemistry" [16,17] or reaction control [18–21] including chiral molecules [22,23]. This question has been addressed from a variety of points of view, and Jörn Manz and his group have been early players in the field, including both bimolecular and unimolecular reactions [24–26]. Mode selective chemistry has been discussed for some very simple systems such as O_3 [27] and H_2O isotopomers as well as other examples [28–33]. Among the important early developments we may mention also the demonstration, on the basis of fs wavepackets derived from high resolution spectroscopic experiment, of mode selective intramolecular vibrational redistribution as a primary process in chemical kinetics [34,35]. Later, femtochemistry has provided experimental examples for

* Corresponding author. Tel.: +41 44 632 44 21; fax: +41 44 632 10 21.
E-mail address: Martin@Quack.ch (M. Quack).
[1] Present address: University of British Columbia, Department of Chemistry, Vancouver, BC, Canada V6T 1Z1.

0301-0104/$ - see front matter © 2007 Elsevier B.V. All rights reserved.
doi:10.1016/j.chemphys.2007.06.012

one-dimensional quantum wavepackets [36,37] as well as multidimensional kinetics of polyatomic molecules in isolation and under condensed phase condition, a development which was well honored as time proceeded [38–41].

It is probably fair to say that much of the impressive progress in this general field was either based on experimental, largely empirical results with little theoretical analysis, or else on very approximate, quantum theoretical analysis, and highly simplified theoretical models. Alternatively there exist accurate quantum theoretical calculations, but in a space of substantially reduced dimensionality, compared to the complete dynamical problem. In a few cases full dimensional quantum calculations on appropriate potential hypersurfaces exist for six-dimensional (4-atom) and nine-dimensional (5-atom) systems. Only classical molecular dynamics of either the empirical force field [42] or the Car–Parrinello type [43] has been able to provide accurate theory for really high dimensional systems, but then with the limitations of the classical approximation for the nuclear degrees of freedom. The possible inclusion of quantum effects in high dimensional simulations has been reviewed recently [44,45].

We have, in recent years, embarked on a study of a few prototypical reaction systems, for which accurate spectroscopic and ab initio results are obtainable as well as a full dimensional quantum dynamical treatment. We may mention in this context as examples on the one hand hydrogen bond dynamics in isotopomers of hydrogen fluoride dimers [46–50] and inversion in Ammonia isotopomers [51–55] and on the other hand stereomutation dynamics in hydrogen peroxide and related systems [56–64]. Hydrogen peroxide in its equilibrium geometry exists in two enantiomeric forms separated by a low torsional barrier (of about 360 cm^{-1}) conventionally labelled the P and M enantiomers (see Fig. 1).

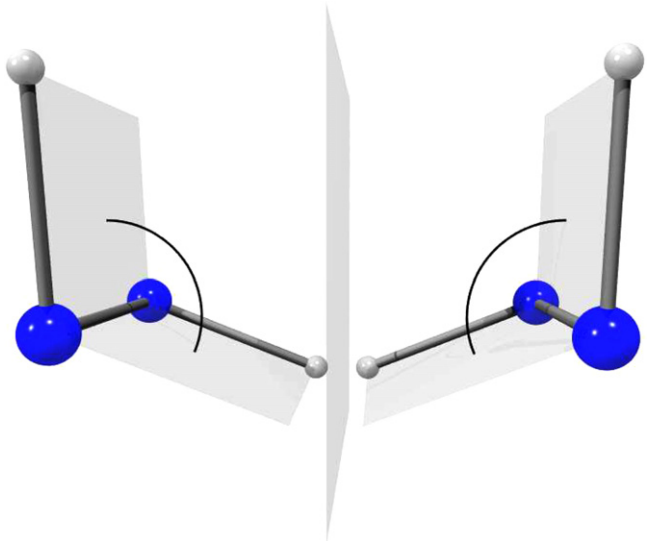

Fig. 1. H_2O_2 in its two enantiomeric equilibrium geometries, P-enantiomer on the left-hand side, M-enantiomer on the right-hand side.

The torsional tunneling is conventionally and quite easily treated in a one-dimensional torsional potential with a low *trans*-barrier (about 360 cm^{-1}) and a much higher *cis*-barrier. For this system we have derived some time ago a semiglobal fully six-dimensional potential energy hyperface in a collaboration of the Lausanne and Zurich groups [56] and we have already presented some quantum dynamical results on this hypersurface [57,64]. The surface has also been used by others for stationary state calculations [65,66]. We may mention here as well that stereomutation tunneling in hydrogen peroxide has also been investigated in relation to the fundamental phenomenon of parity violation in chiral molecules [67–69]. Indeed, hydrogen peroxide has been a prototype molecule for theoretical calculations of molecular parity violating potentials (see [67–71] and the reviews [72,73] for further references). We have discussed the importance of the interplay of parity violation with tunneling dynamics in this context [58–63,72,73].

The aim of the present paper is to provide a more complete report of our results on the time dependent multidimensional quantum tunneling wavepackets dynamics. We shall address the following main questions in this context:

1. How is the stereomutation tunneling visible in multidimensional wavepackets and how is it affected by excitation of various vibrational modes in the multidimensional space, perhaps in a mode selective or a statistical fashion?
2. What is the nature of the wavepacket motion in quasi-adiabatic above barrier tunneling?
3. Are there useful approximations of reduced dimensionality, which provide an adequate description in relation to the full dimensional quantum dynamical results?
4. How can one understand the emergence of relaxation and racemisation in thermal systems as opposed to periodic tunneling stereomutation?

2. The potential hypersurface and theoretical methods

We summarize here only briefly the main methods used in our work, as the potential hypersurface and numerical methods have been described in some detail before [56,57,64,74]. The potential hypersurface used here is the PCPSDE function derived in [56]. It provides an analytical description of the potential V as a function of the bond lengths $R = R_{OO}$, $r_1 = r_{O_1H_1}$ and $r_2 = r_{O_2H_2}$ with obvious notation for the two hydrogen atoms numbered H_1 and H_2 and the two oxygen atoms numbered O_1 and O_2. The three angles used are θ_1 as angle between the bonds H_1–O_1–O_2 and θ_2 between the extended O_1–O_2 vector and O_2–H_2 bond. The particularly important torsional angle τ is given by the angle between the H_1–O_1–O_2 plane and the O_1–O_2–H_2 plane. The potential hypersurface was derived from a set of pointwise ab initio calculations and then adjusted to a selected set of experimental data, which

included structural parameters and the torsional barrier (360 cm^{-1} for the lower *trans*-barrier) and the dissociation energies D_0 for the simple bond fission $H_2O_2 \rightarrow 2OH$ (giving $D_e = 19{,}039\ cm^{-1}$) as well as a number of other data. While the surface was not fitted to spectroscopic accuracy in [56], it describes many important properties of H_2O_2 within reasonable accuracy (see [56] for a detailed discussion). For the present study it is particularly relevant that the experimental ground state tunneling splitting was accurately described already by fully six-dimensional quantum Monte Carlo calculations for the three isotopomers HOOH, HOOD and DOOD in the original adjustment of the surface, and subsequently confirmed by several fully six-dimensional discrete variable representation (DVR) calculations [56,57,64–66]. Also the interaction of tunneling with various vibrational excitations is well described, as far as comparison to experiment is possible [57]. We may note that the analytical semiglobal PCPSDE potential hypersurface was in part based on a set of ab initio points calculated at an intermediate level of accuracy (CASPT2, etc.), to start with. A balanced choice of quantum chemical methods was necessary in order to describe large portions of the hypersurface including bond extensions corresponding to high overtone excitations and dissociation channels. For a detailed discussion of the philosophy used in deriving such a semiglobal hypersurface we refer to [56]. A somewhat different strategy was used in the work of Koput, Carter and Handy [75,76], where higher level quantum chemical calculations were used (CCSD(T)) to derive a more local force field, accurate for amplitudes of motion corresponding to low energies [75,76]. While higher accuracy has been claimed for this low energy part of the surface [76], the differences are actually not very large and the local surface does not give an accurate description of high excitation energies.

In order to describe the time dependent dynamics on the surface we have followed a two step procedure, by first solving the time independent Schrödinger equation numerically (exactly)

$$\hat{H}\psi_n(q_1,q_2,q_3,q_4,q_5,q_6) = E_n\psi_n(q_1,q_2,q_3,q_4,q_5,q_6) \qquad (1)$$

in a discrete variable representation (DVR). We used the generalized coordinate DVR described in detail in [64]. In terms of generalized vibrational coordinates q_k and their conjugate momenta $\hat{p}_k = -i\hbar\partial/\partial q_k$ the Hamilton operator $\hat{H}$ is given by Eq. (2):

$$\hat{H}/(hc) = \frac{1}{2hc}\left(\sum_{k,l=1}^{6}\hat{p}_k G_{k,l}\hat{p}_l\right) + V(q_1,q_2,q_3,q_4,q_5,q_6), \qquad (2)$$

$V(q_1,q_2,q_3,q_4,q_5,q_6)$ is the effective potential energy including contributions from the mass-dependent pseudopotential [74]. The $G_{k,l}$ are generalized Wilson G-matrix elements, which one might call "effective inverse reduced masses". An important feature of the generalized DVR approach [64] is the completely numerical evaluation of all terms arising in Eq. (2) including the $G_{k,l}$ and the pseudopotential. The Hamiltonian is diagonalized in a Chebychev DVR obtained by mapping the generalized coordinates q_k onto equidistant grids. This mapping leads to additional contributions to the $G_{k,l}$ [64]. In the present work, we have used the valence coordinates mentioned above, usually with linear mappings except for the treatment of very high OH stretching excitations, where nonlinear mappings of the two OH bond lengths allowed to account for large bond elongations without unduly increasing the number of grid points [64]. Appropriate truncation of the full rectangular grid leads to a DVR-Hamiltonian with about 10 million basis functions. Extensive successive truncation [64,74,77] in all six degrees of freedom allows for the efficient computation of the lowest few hundred eigenvalues with adequate accuracy. For a more detailed discussion of the DVR calculations and their convergence we refer to [57,64] as well as to comparison with subsequent results by other groups [65,66,78].

We can expect sufficient accuracy of these calculations as well as the underlying potential surface to be able to claim essentially quantitative validity to within reasonable experimental accuracy for the wavepacket results reported below. The level of accuracy reached can be judged from comparison with spectroscopic experiment, where available.

In addition to the full-dimensional numerical DVR-solution of the time independent problem, we have also used an approximate adiabatic separation of the torsional degree of freedom [57,64,74]. In essence we use a quasiadiabatic channel reaction path Hamiltonian (RPH) approach with the reaction path coordinate q being described by a torsional motion with the angle τ. This defines a Hamiltonian operator $\hat{H}_q(\hat{p},q)$, which depends upon q and the conjugate momentum $\hat{p}$. The full Hamiltonian is approximated by including a second term with a parametric dependence upon q following Eq. (3):

$$\hat{H}(\hat{p},q,\boldsymbol{P},\boldsymbol{Q}) = \hat{H}_Q(\boldsymbol{P},\boldsymbol{Q};q) + \hat{H}_q(\hat{p},q). \qquad (3)$$

The $\boldsymbol{Q}$ and $\boldsymbol{P}$ describe all coordinates and momenta in the set of $3N-7$ remaining degrees of freedom. The wavefunction is approximately given by the product wavefunction in Eq. (4):

$$\Psi^n_m(\boldsymbol{Q},q) = \chi^n_m(q)\phi_n(\boldsymbol{Q};q), \qquad (4)$$

where the $\chi^n_m(q)$ are the eigenfunctions associated with the adiabatic channel n

$$(\varepsilon^n(q) + \langle\phi_n|\hat{H}_q|\phi_n\rangle - E^n_m)\chi^n_m(q) = 0. \qquad (5)$$

In the quasiharmonic, quasiadiabatic approximation the ϕ_n are furthermore approximated by a product of harmonic oscillator functions β

$$\phi_n(\boldsymbol{Q},q) = \prod_{k=1}^{3N-7}\beta^{n_k}_k(Q_q;q). \qquad (6)$$

However, more generally the $\phi_n(\boldsymbol{Q};q)$ may be anharmonic vibrational wavefunctions. We have described details of the theory and methods before [57,64,74]. The technique follows closely the work of Miller, Handy and Adams [79], which itself can be related to earlier models using vibrationally adiabatic separations (see [80–87] and refer-

ences cited therein). An important modification in our work is the elimination of non-physical avoided crossings of channels by a strictly speaking "diabatic" (hence "quasiadiabatic") approach. The physical idea behind this is to generate quasiadiabatic channel wavefunctions which behave smoothly along the reaction path thus allowing for real crossings instead of avoided crossing. The spirit is very similar to the allowance for such physically motivated crossings in the adiabatic channel model [84]. This can be realized simply by a sequence of "2×2 diabatic rotations" [57]. As a reference point for the diabatic rotations we choose the channel energies at the equilibrium value of the torsional angle (about 110°, see also [64]). Fig. 2 illustrates the consequences of this procedure for the 150 lowest channels for H_2O_2: On the left-hand side we show the strictly adiabatic channels and on the right-hand side ($\tau \geqslant 180°$) the corresponding quasiadiabatic channels after 20,000 diabatic rotations. One can very nicely see the important effect of this procedure, which in practice allows for generating an efficient and quite good approximation for the total wavefunctions and relative energies (in particular tunneling splittings). As is clear from Fig. 2 the effect on RPH results will be very small for the lowest channels in the case of H_2O_2, but for higher excitations (Fig. 5) strictly adiabatic results without diabatic rotations would be unphysical. Fig. 2 also illustrates the rather large density of channels for even a small molecule such as H_2O_2. Fig. 3 shows as a further illustration the torsional wavefunctions supported by the adiabatic channel corresponding to the antisymmetric bending fundamental ν_6 (within the RPH model).

Finally, we have obtained solutions of the time dependent Schrödinger equation in the eigenstate basis, hence

$$i\hbar \frac{\partial \Psi(q_1, q_2, q_3, q_4, q_5, q_6, t)}{\partial t} = \hat{H} \Psi(q_1, q_2, q_3, q_4, q_5, q_6, t) \tag{7}$$

with the time evolution operator $\hat{U}(t, t_0)$

$$\Psi(q_1, q_2, q_3, q_4, q_5, q_6, t) = \hat{U}(t, t_0) \Psi(q_1, q_2, q_3, q_4, q_5, q_6, t_0), \tag{8}$$

$\Psi(q_1, q_2, q_3, q_4, q_5, q_6, t_0)$ was chosen to satisfy certain predefined initial conditions, such as well defined chirality, implying strict localization in a subspace of τ. Of course, in the eigenstate basis $\Psi(q_1, q_2, q_3, q_4, q_5, q_6, t)$ can be equivalently generated from the eigenfunctions of $\hat{H}$

$$\Psi(q_1, q_2, q_3, q_4, q_5, q_6, t) = \sum_{n=0}^{\infty} c_n \psi_n(q_1, q_2, q_3, q_4, q_5, q_6) \times \exp(-2\pi i E_n t/h). \tag{9}$$

The initial condition in this representation simply defines the time independent coefficients c_n. As we have discussed

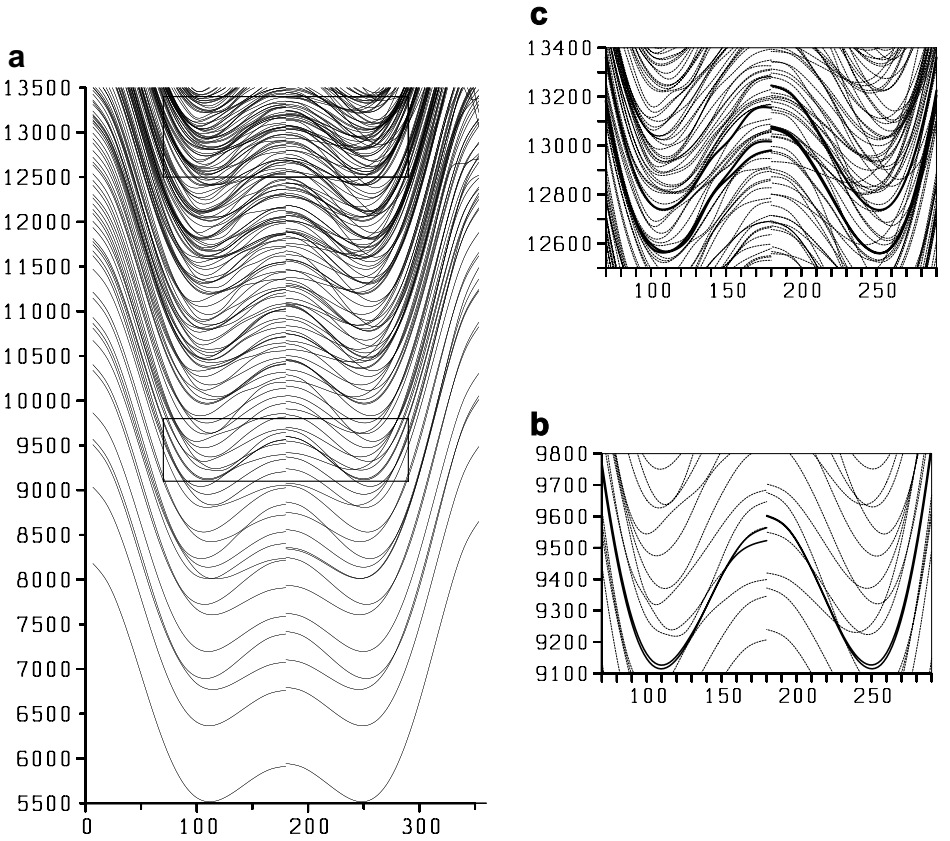

Fig. 2. The effect of diabatic rotations on the torsional channel potentials. The ordinate scale gives the potential energies E/hc, in cm^{-1}, the abscissa gives the torsional angle τ in degrees. For $\tau \leqslant 180°$ we show the strictly adiabatic channel potentials. For the symmetrically equivalent space $\tau \geqslant 180°$ we show the quasiadiabatic channels resulting after 20,000 diabatic rotations. (a) The lowest 150 channels for H_2O_2. (b) Detail of the two channels corresponding to the OH stretching fundamentals (bold lines) surrounded by other channels. (c) Detail of the three channels corresponding to the first OH stretching overtone levels (bold lines) embedded in numerous other channels.

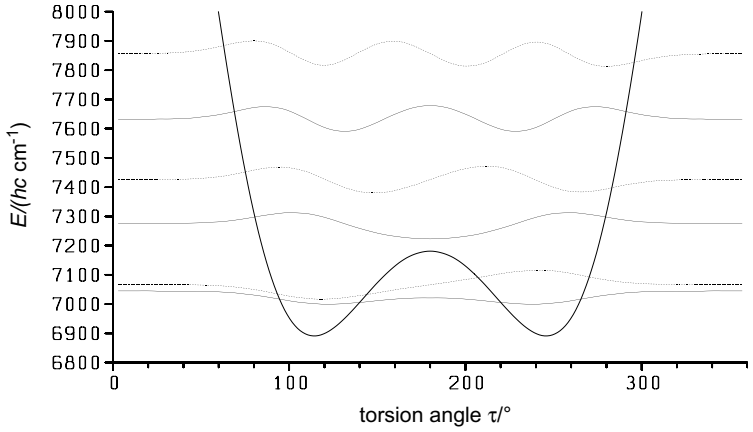

Fig. 3. The lowest torsional wavefunctions supported by the adiabatic channel corresponding to the antisymmetric bending fundamental v_6 (calculated with the RPH model). Full lines: Wavefunctions of positive parity (+). Dotted lines: Wavefunctions of negative parity (−). The ordinate axis labels refer to the energies $E/(hc\ \mathrm{cm}^{-1})$, the wavefunctions are shown without scale for illustration, centered at the positions of the corresponding energy levels.

elsewhere, this approach has obvious advantages, when deriving dynamics from high resolution spectroscopy, where the ψ_n and E_n are needed anyway in the adjustment to experimental data. The approach has also advantages for the treatment of multiphoton excitation with coherent monochromatic radiation, as long as the coupling to the coherent radiation field is not too strong (see [10–13] for a discussion). In the present work we restrict our attention to purely intramolecular non radiative short time dynamics.

Finally, for graphical illustration of the results we have calculated the probability density in the torsional coordinate τ by explicit representation of the wavefunction in the internal coordinates and integration over the complete space for all coordinates except τ. hence

$$|\Psi(\tau,t)|^2 = \int \cdots \int |\Psi(r_1,r_2,R,\theta_1,\theta_2,\tau,t)|^2\, \mathrm{d}r_1\, \mathrm{d}r_2\, \mathrm{d}R\, \mathrm{d}\theta_1\, \mathrm{d}\theta_2. \tag{10}$$

where we use the common "Podolski weighting" of the wave functions.

3. Results and discussion

3.1. Eigenstate spectrum, tunneling splittings and times

Table 1 summarizes results for vibrational fundamentals, tunneling splittings $hc\,\Delta\tilde{\nu}_\pm = \Delta E_\pm$ and tunneling times $\tau_{\lambda\to\rho}$ with excitation of the corresponding fundamentals. The tunneling times were calculated with the usual two level equation

$$\tau_{\lambda\to\rho} = \frac{h}{2\Delta E_\pm} = \frac{1}{2c\Delta\nu_\pm}, \tag{11}$$

where $\Delta E_\pm$ is the separation of levels of positive and negative parity supported on the channel with a given fundamental excitation v_i, as shown for the example of v_6 in Fig. 3. For experimental results or exact DVR results one would simply take the splittings from appropriately assigned adjacent vibrational levels of different parity and we shall discuss the physical significance in more detail in Section 3.2.

The tunneling splittings as a function of vibrational excitation in H_2O_2 have found recent attention using a variety of methods and potentials. Several authors used in fact the PCPSDE potential from our work. Table 2 summarizes these results for convenience, to show the overall consistency, when the same potential is used, but also some differences when using different potentials. The general agreement is actually quite good.

Fig. 4 shows the tunneling splittings for fundamentals and combination tones as a function of vibrational energy up to about 4000 cm^{-1}. At first sight these generate the impression of an almost random distribution scattered in the range between about 4 cm^{-1} and 50 cm^{-1} around the ground state tunneling splitting of about 11 cm^{-1}, and we shall return to this point in Section 3.3. The apparently "random" distribution in Fig. 4 arises fairly systematically by combining the effects from catalyzing and inhibiting modes. The only mode strongly catalyzing tunneling stereomutation is the antisymmetric O–O–H bending v_6 and from the assignments one sees the effects of increasing excitation in v_6, which defines an almost straight line as a function of v_6 in the upper part of the figure, and from the combination with other modes. The mode v_3 is an almost inactive "spectator" mode, which leaves tunneling unchanged, except for a slightly catalyzing effect at higher excitation. This leads to two slightly increasing sets of splittings with energy for the series 3_1, 3_2, 3_3, 3_4 and 3_16_1, 3_26_1, 3_36_1 in Fig. 4, where we have used the vibrational symbol convention of [94].

All other modes are, in fact, inhibiting stereomutation tunneling. The most strongly inhibiting mode is the symmetric OOH bending mode v_2. Increasing its excitation leads to a systematic decrease of the tunneling splitting. Combining v_2 and v_6 excitation in 2_16_1 one finds almost complete compensation of the inhibiting and the catalyzing

Table 1
Energy levels and tunneling times for various fundamental excitations in H_2O_2 on the PCPSDE surface of [56]

i	ω_i (cm^{-1})	$\tilde{\nu}_i$ (cm^{-1})		$\Delta\tilde{\nu}_i$ (cm^{-1})			
		Exp[a]	6D	Exp[a]	6D	RPH	$\tau_{\lambda\to\rho}$ (ps) (6D)
0	[5786]		[5691.7]	11.4	11.0	11.1	1.5
1	3778	3609.8 (3605?)	3617.7	8.2	7.6	8.4	2.2
2	1453	1395.9	1392.0	(2.4?)	6.1	5.0	2.7
3	889	865.9	850.5	12.0	11.1	10.8	1.5
4	392	254.6	259.3	116.	118	120.	0.14
5	3762	3610.7	3605.8	8.2	7.4	7.4	2.0
6	1297	1264.6	1236.5	20.5	20.8	21.8	0.8

[a] Experimental data from [88–93]. Note that in [57] the labels of ν_1 and ν_5 were interchanged.

Table 2
Tunneling splittings $\Delta\nu_i$ for H_2O_2 derived by various dynamical approximations and potentials for vibrational fundamentals ν_i

Mode ν_i	FLQ[a]	RPH[a]	(4 + 2)D[b]	GCDVR[c]	CMG[d]	PIA[e]	H[f]
ν_0	11.0	11.1	11.3	11.0	11.0	11.3	11.2
ν_1	7.6	8.4	(7.7)	7.6	7.6	9.4	10.2
ν_2	6.1	5.0	6.6	6.4	6.1	6.3	6.3
ν_3	11.1	10.8	11.3	11.1	11.0	11.6	11.6
ν_4	118	120	120.4	118.9	118.9	115.8	–
ν_5	7.4	7.4	(7.7)	7.4	7.3	8.7	8.7
ν_6	20.8	21.8	21.5	20.8	20.75	21.2	19.3

The results in columns 2–6 are all based on the PCPSDE surface of Ref. [56], whereas columns 7 and 8 give results from independent calculations on different potentials.
[a] Ref. [57].
[b] Ref. [56].
[c] Ref. [64].
[d] Ref. [65].
[e] Perturbative instanton approach [78].
[f] Ref. [93].

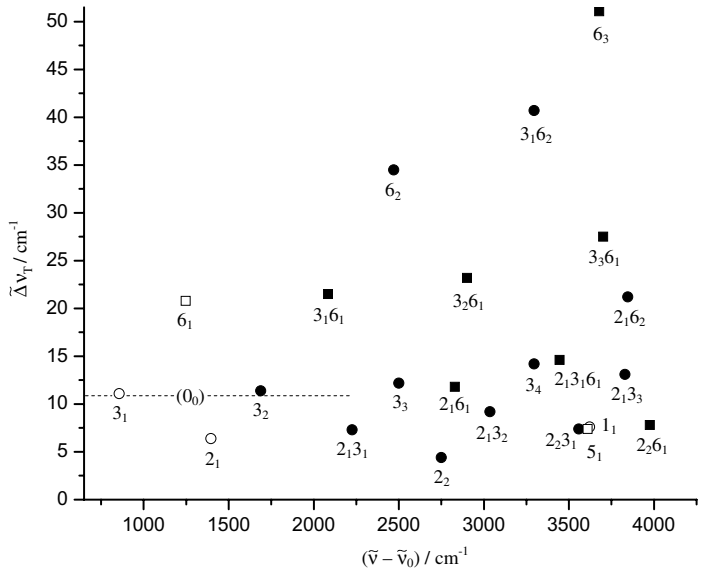

Fig. 4. Calculated torsional tunneling splittings $\Delta\tilde{\nu}_T$ as a function of vibrational excitation in the other modes ($\nu_1, \nu_2, \nu_3, \nu_5, \nu_6$) obtained from the exact six-dimensional DVR calculations. The abscissa gives the average excitation above the ground level $v = (v_+ + v_-)/2$ for each tunneling pair. Open symbols refer to fundamentals, full symbols to combinations and overtones. Circles are for levels with A-symmetry, squares for levels with B-symmetry. The assignment of the level is described by giving the mode X with its vibrational quantum v_X as right index. Modes in the ground level are not indicated. Thus $2_1 3_1 6_1$ implies one quantum of vibration in each of the modes ν_2, ν_3 and ν_6 and zero quantum in all other modes (see [94] for this convention). The position of the ground state tunneling splitting is given by a dashed line marked 0_0 for the ground state.

effects. The results shown in Fig. 4 can thus rather easily be rationalized by a combination of catalyzing and inhibiting effects from the different vibrational modes. It should be made clear that all results discussed in Fig. 4 correspond

to the torsional ground level doublet. If the torsional mode itself is further excited, then the splitting increases much more strongly, beyond the range shown in Fig. 4. One might also note that in a strictly separable picture all results in Fig. 4 would fall on a line parallel to the abscissa with the ground state splittings, which is indicated as a dashed line in the figure (marked 0_0). The effects result from a quasiadiabatic interaction of the torsional doublet with the various modes.

Both of the two OH stretching modes v_1 and v_5 are inhibiting tunneling. A further question thus refers to the systematic decrease of the tunneling splitting with increasing OH stretching excitation to very high energies. This has found experimental interest for quite some time, and has also been addressed theoretically by us before [56,64]. Fig. 5 shows the results for various OH stretching polyad levels, where $N = v_1 + v_5$ is the polyad quantum number. One sees the dramatic decrease of the stereomutation rate $\tau^{-1} = \Delta E/h$, demonstrating the inhibiting character of OH stretching.

We conclude this section by giving the results for the spectrum of the torsional mode itself in the $(5+1)$-dimensional adiabatic calculation, which singles out this coordinate as reaction coordinate, and thus allows the assignment of torsional levels, in Table 3. While for the lowest levels the $(5+1)$-dimensional results are accurate, within 0.1 cm^{-1} of the six-dimensional results, for higher excitation the error increases to 10 cm^{-1} and even several 10 cm^{-1} at the highest levels. One observes the convergence to the free rotor degeneracy at the highest levels. The approximate $(5+1)$-dimensional calculations have some merit in formulating a consistent transition state approximation (see Section 3.3).

The reversal of the ($v_T(h) = 7$, A^-, $v_T(l) = 15$) and the ($v_T(h) = 8$, A^+, $v_T(l) = 16$) state energies in the fully coupled six-dimensional result compared with the adiabatic calculations corresponds to an overlap of the $v_T(h) = 7$ and 8 tunneling pairs. This can be the result of a local resonance, which is an inherently non-adiabatic effect. In principle, such effects are not too surprising, as the (A^-/A^+) splitting is less than the inverse vibrational density of states at this energy since we are close here to the limit of almost free rotation, where $v_T(h) = 7$, A^- becomes almost degenerate with $v_T(h) = 8$, A^+ (see Table 3). Fig. 6 gives a graphical survey of the lowest adiabatic channel potential related to the torsional level positions from the $(5+1)$-dimensional adiabatic channel calculations up to the energy of the *trans*-barrier.

Table 3
Spectrum of the torsional mode in the $(5+1)$ adiabatic approximation and quantum numbers in both low$^{(l)}$ and high$^{(h)}$ barrier notation (first and second columns)

$v_T(l)$	$v_T(h)$	Γ	$\tilde{\nu}$[a] (cm^{-1})	$(\tilde{\nu}-\nu_0)$[a] (cm^{-1})	$(\tilde{\nu}-\nu_0)$[b] (cm^{-1})
0	0	A^+	175.8	0	0
1	0	A^-	186.9	11.1	11.0
2	1	A^+	435.4	259.6	259.3
3	1	A^-	554.8	379.0	378.2
4	2	A^+	758.3	582.5	580.9
5	2	A^-	971.8	796.1	792.8
6	3	A^+	1204.4	1028.6	1023.7
7	3	A^-	1447.8	1272.0	1225.0
8	4	A^+	1697.2	1521.4	1513.7
9	4	A^-	1950.6	1774.9	1761.2
10	5	A^+	2192.5	2016.7	2005.1
11	5	A^-	2454.3	2278.5	2262.0
12	6	A^+	2612.1	2436.3	2423.9
13	6	A^-	2967.5	2791.7	2766.8
14	7	A^+	3000.5	2824.7	2797.8
15	7	A^-	3541.3	3365.5	3326.4
16	8	A^+	3543.7	3367.9	3318.0
17	8	A^-	4204.2	4028.4	3962.1

[a] The wavenumber $\tilde{\nu}$ is given with respect to the minimum of the lowest adiabatic channel. This minimum is 5516 cm^{-1} above the minimum of the potential hypersurface. The *trans*-barrier in the channel is at 5913.4 cm^{-1} (397.3 cm^{-1} above its minimum). The total zero point energy is 5691.9 cm^{-1} in the $(5+1)$-dimensional adiabatic approximation (5691.7 cm^{-1} exact six dimensional).

[b] Six-dimensional result.

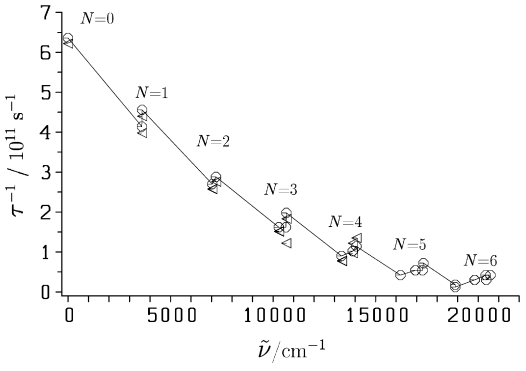

Fig. 5. Stereomutation period τ (represented as $\tau^{-1} \propto$ tunneling splitting) as a function of the OH stretching excitation, calculated from an adiabatic approximation. Circles show results using a basis with pure OH stretching excitation ($v_2 = v_3 = v_4 = v_6 = 0$). Triangles show results including some OH bending excitation in the basis functions ($v_3 = v_4 = 0$ and $0 \leqslant v_2 + v_6 \leqslant 2$). $\tilde{\nu}$ is the excitation wavenumber above the zero point level.

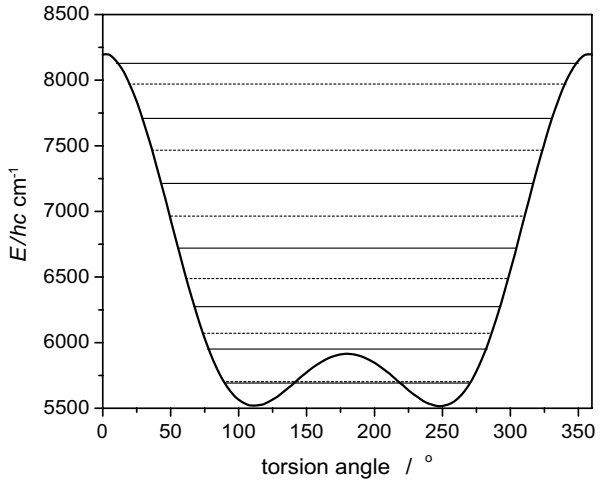

Fig. 6. Lowest adiabatic channel potential and torsional levels from the $(5+1)$-dimensional adiabatic channel calculations.

3.2. Results on stereomutation wavepackets

The most common spectroscopic analysis of tunneling, indeed, relates observed 2-level splittings to periodic interconversion rate processes by means of Eq. (11). There is an implicit assumption in such an analysis, which is not always clearly appreciated or stated: The wavefunction associated with the two levels showing the observed splitting ΔE must be such that the motion described by the two term approximation applied to Eq. (9) corresponds to the process for which one wishes to infer the rate. In fact, any chosen pair of levels in the sum of Eq. (9) will exhibit a periodic time evolution given by Eq. (11), however, usually with some physics very different from, say, a process of stereomutation. This question relates to the problem of the proper spectroscopic (or theoretical) *assignment* of the observed pair of levels, which really implies the proper understanding of the molecular wavefunctions associated with the levels. For ground state tunneling splittings such an assignment and at least a qualitative understanding of the associated wavefunctions is usually straightforward, although even there one may have exceptions to the rule and some pitfalls. For excited states the corresponding problem can be highly nontrivial and in particular for above barrier tunneling to be discussed below, the wavefunctions might be very complicated and not correspond to a simple process. For example the adiabatic channel for $v_6 = 1$ shown in Fig. 3 supports two "tunneling wavefunctions" highly above the barrier of the lowest quasiadiabatic channel, which it exceeds by more than 1000 cm^{-1}. If the quasiadiabatic channel RPH picture shown in Fig. 3 is correct, then indeed the two lowest wavefunctions shown there are associated with a tunneling splitting which gives a simple stereomutation process. More generally, a multidimensional wavepacket analysis is necessary to obtain firm conclusions and we shall present here such an analysis in an exemplary fashion.

Fig. 7 shows such a result for a multidimensional time dependent probability density, represented in one dimension following Eq. (10), at the ground state energy. The initial wavepacket at $t = 0$ was strictly localized on one side of the barrier (at $\tau < 180°$) and then propagated following Eq. (8). One finds, indeed, the expected periodic wavepacket motion with a period of about 3 ps, which continues for hundreds of picoseconds in an essentially unperturbed manner as shown. In the vapor phase at atmospheric pressure collisions will interfere after about 1 ns and at low pressure thermal background radiation will interrupt the process at much longer times.

Fig. 8 shows the time dependent wavepacket result with an initially strictly localized, chiral wavepacket (for $\tau \leqslant 180°$ only at $t = 0$) and at the same time one quantum of vibrational excitation in the antisymmetric O–O–H bending mode v_6 at 1236 cm^{-1}. Given a torsional *trans*-barrier at 360 cm^{-1} its excitation is well above the energy needed for almost free internal rotation. However, while the period of motion is reduced by about a factor of two,

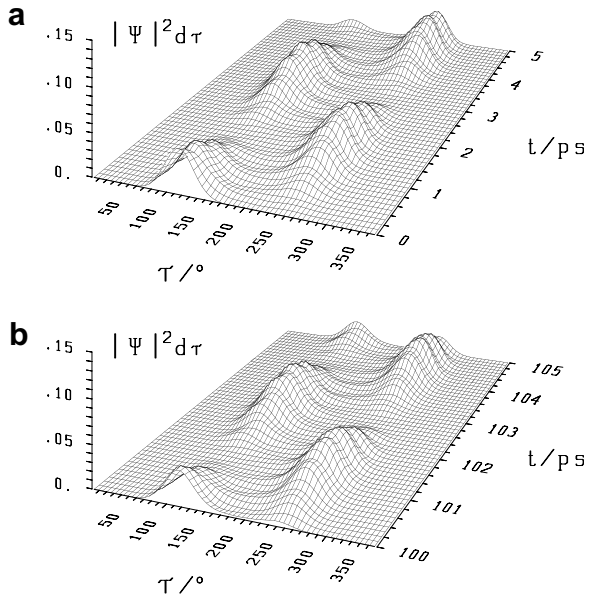

Fig. 7. Six-dimensional wavepacket evolution in H_2O_2. $|\Psi|^2\,d\tau$ shows the time dependent probability as a function of the torsional coordinate, integrating the probability density over all other coordinates as defined by Eq. 10. (a) Shows the first 5 ps with an initial distribution localized on one side of the torsional barrier ($0 \leqslant \tau \leqslant 180°$) at the ground state energy, roughly corresponding to a superposition of the lowest A^+ and A^- tunneling levels. (b) The time range 100–105 ps with the initial condition at $t = 0$ as in (a).

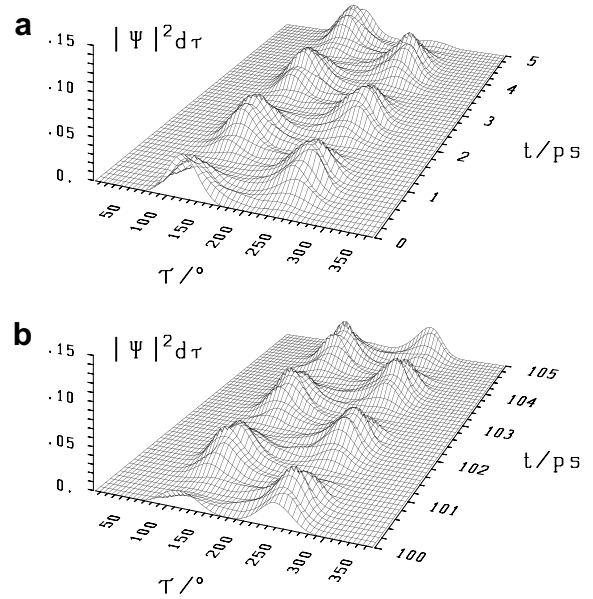

Fig. 8. Six-dimensional wavepacket dynamics in H_2O_2 from exact six-dimensional DVR results with an initial condition including excitation with one quantum of the catalyzing antisymmetric OOH bending mode ($v_6 = 1$), otherwise as in Figs. 6 and 7.

its structure in the six-dimensional space at energies high above the barrier remains that of an essentially periodic tunneling wavepacket, very similar to the ground state tunneling well below the barrier. Of course this is anticipated

from the good validity of the quasiadiabatic channel RPH approximation, which was *not* used for the results in Fig. 8 which shows the numerical DVR solution for the fully coupled six-dimensional Hamiltonian. This phenomenon of quasiadiabatic above barrier tunneling is fairly ubiquitous and provides the basis for the spectroscopic analysis of mode selective tunneling dynamics [46–55]. In the present example OOH bending is a "catalyzing mode", whose excitation speeds up the tunneling process, but other modes slow down the stereomutation by quasiadiabatic above barrier tunneling, in the case of OH stretching very much so, as we have seen above. One notes in Fig. 8 that for very long times of 100 ps the changes in the wavepacket are somewhat larger than for ground state tunneling in Fig. 6, but they remain rather unimportant.

Fig. 9 provides an interesting test for the use of the quasiadiabatic channel RPH approximation in solving the time dependent Schrödinger equation for multidimensional tunneling. The close similarity of the results in Figs. 9 and 8 show the RPH model to be excellent for this example, and Table 1 suggests that it is of similar quality for other excitations in H_2O_2. This is excellent news for treating multidimensional tunneling in molecules similar to H_2O_2 but possibly also much more complex systems such as Aniline (and its isotopomers, in particular the chiral isotopomers C_6H_5NHD), where we have already applied the approach to spectroscopic results from our work [74,95].

Fig. 10 shows snapshots of two-dimensional probability densities obtained from the full six-dimensional densities by integration over all coordinates except torsion and OOH bending. Here one can compare the ground state and excited state $v_6 = 1$ wavepackets. Essentially in the second case one has a quasistationary excited state density (for $v_6 = 1$) which is propagated in the torsional coordinate by the quasiadiabatic above barrier tunneling.

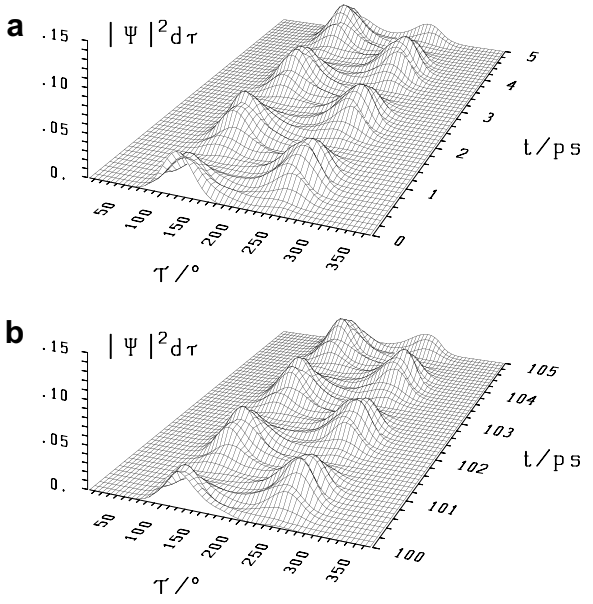

Fig. 9. Six-dimensional wavepacket dynamics in H_2O_2 calculated with the quasiadiabatic channel RPH approximation and one quantum of OOH bending ($v_6 = 1$), conditions otherwise as in Figs. 7 and 8. There is only a slight phase shift visible compared to Fig. 8.

One notes again the increased tunneling rate in $v_6 = 1$ compared with the ground state, which is a peculiarity of v_6, whereas v_1, v_2 and v_5 excitation would slow down the tunneling process. We refrain here from showing these and other examples as the conclusions are similar and fairly obvious. In all these excitations tunneling proceeds with increased or reduced rate but otherwise almost unperturbed, very similar to ground state tunneling, by a process which may be justly called quasiadiabatic above barrier tunneling because of the effective vibrationally adiabatic separation of these vibrational modes from torsion.

3.3. Stereomutation wavepackets and multistate racemisation with random, quasithermal initial conditions

After we have discussed in the previous sections results for tunneling and wavepacket motion with certain selected initial excitations involving few states we turn now to wavepackets with "random" initial excitations, involving very many states, in order to illustrate the situation corresponding to a thermal reaction. The initial state vector at $t = 0$ in Eq. (9) is chosen in such a way, that it is always localized on one side of the potential barrier ($0 \leqslant \tau \leqslant 180°$) and that the populations $p_n = |c_n|^2$ are randomly drawn from a Boltzmann distribution at some temperature T and with the complex phase angles α_n in $c_n = |c_n|\exp(i\alpha_n)$ being drawn randomly from the interval $0 \leqslant \alpha_n \leqslant 2\pi$. For a detailed discussion for such "quasithermal quantum mechanical trajections" we refer to [96,97]. One may physically think of randomly drawing a single H_2O_2 molecule from a thermal ensemble, but with the localized initial conditions as specified above.

Fig. 11 shows results for the time evolution of the probability density as a function of the torsional angle τ and as a function of time with initial conditions simulating vibrational–torsional temperatures of 298 K and 700 K for H_2O_2 (without rotation, see below). One can clearly see the damping out of the oscillations at higher temperatures, corresponding to increasingly "random" motion of the probability density.

One can analyse the wavepacket motion in terms of another even more coarse grained variable instead of the detailed probability density $|\Psi(\tau,t)|^2$: the probability of finding either a "left handed" chiral structure $P(M)$ or a "right handed" structure $P(P)$. Clearly the probabilities are just the integrals over the appropriate part of space

$$P(M) = \int_0^{\pi} |\Psi(\tau,t)|^2 \, d\tau = 1 - P(P). \tag{12}$$

Such a result is shown in Fig. 12. It shows the transition from a purely oscillatory stereomutation tunneling at $T = 0$ K to an increasingly damped oscillation. The ordinate in Fig. 12 actually presents what one might call the chiral observable "chirality" of the wavepacket

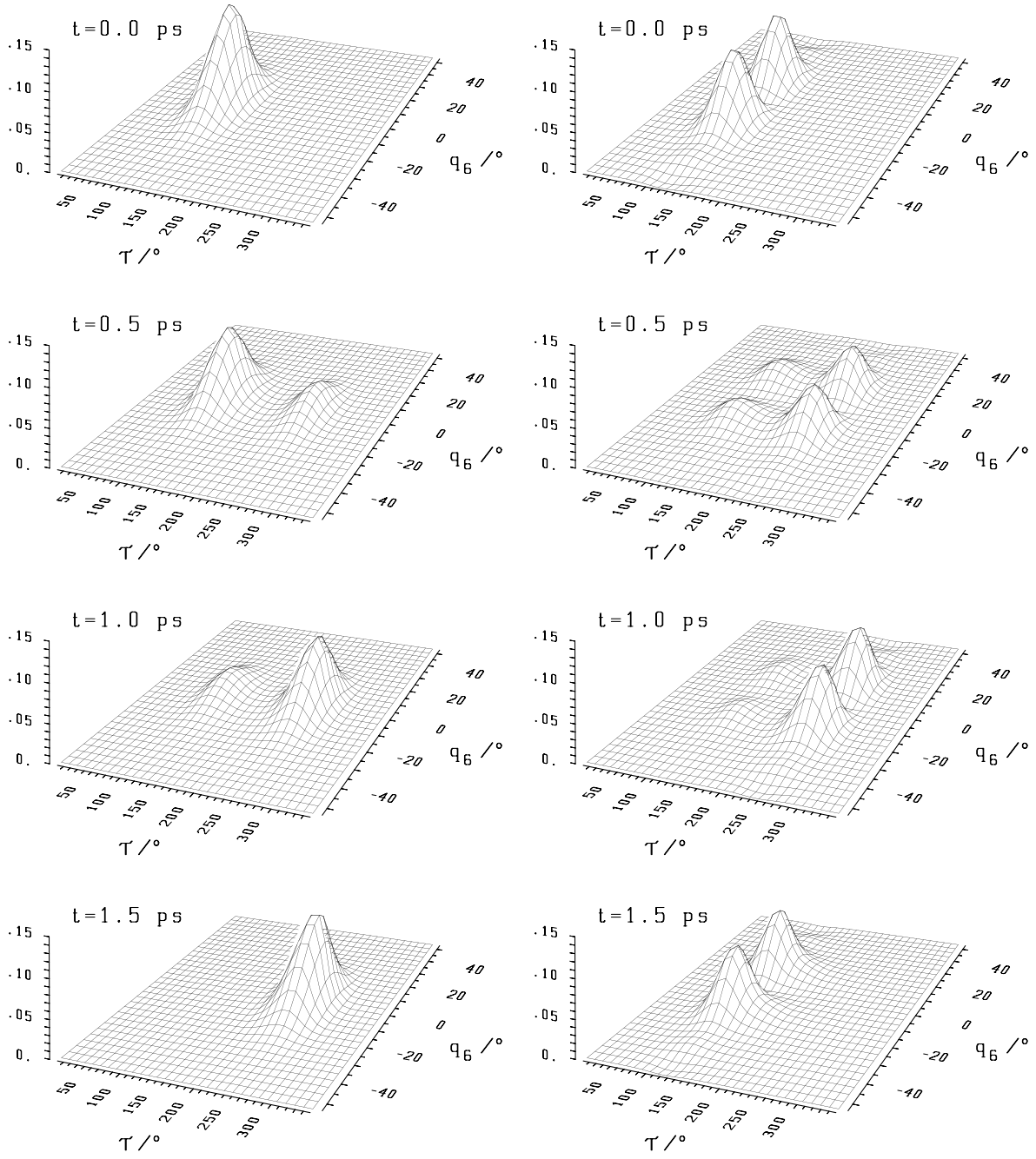

Fig. 10. Six-dimensional wavepacket dynamics in H_2O_2 from exact six-dimensional DVR results. The initial condition is as in Figs. 6 and 7. The ordinate (z) shows the probability density $|\Psi|^2$ integrated over four degrees of freedom as snapshots for certain times as indicated (0–1.5 ps) and as a function of the torsional angle τ (x-axis) and the OOH bending angle (y-axis). Left-hand side for ($v_6 = 0$), right-hand side for ($v_6 = 1$).

$$\chi = P(M) - P(P) \tag{13}$$

which is identical to the frequently used enantiomeric excess (with concentrations C)

$$e_e = \chi = \frac{P(M) - P(P)}{P(M) + P(P)} = \frac{C(M) - C(P)}{C(M) + C(P)}. \tag{14}$$

Of course, one could as well calculate other chiral observables from the full six-dimensional probability density, such as optical activity or optical rotatory power, circular dichroism or vibrational circular dichroism or Raman optical activity, whose behaviour can be related to the time dependent wavefunctions and probability densities by the appropriate time dependent expectation values. Under completely thermalized collisional conditions one would expect simple relaxation towards an equilibrium with $\chi = 0$ (neglecting parity violation). While this is not observed for the collision free random ensemble, the long term oscillation is increasingly damped with increasing temperature and Figs. 13 and 14 show how such a simple relaxation behaviour is approached at a vibrational temperature of $T = 3000$ K where one has a relaxation time

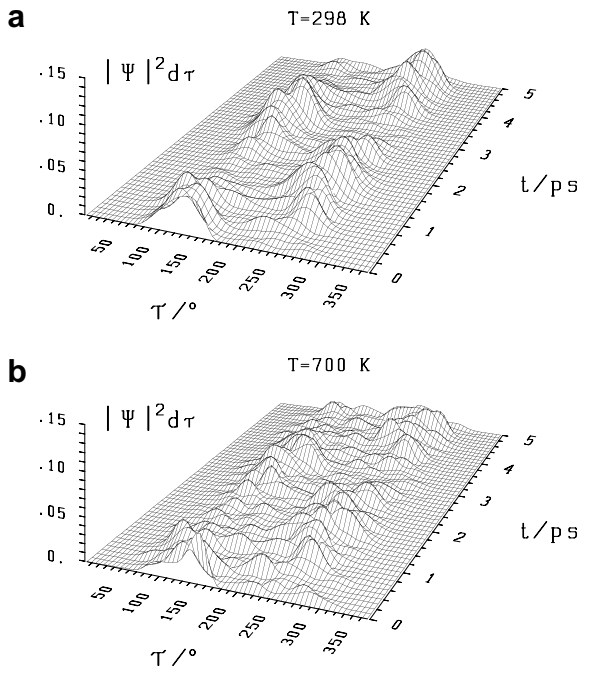

Fig. 11. Six-dimensional wavepacket dynamics in H_2O_2 for initial states with a quasithermal population of levels: (a) for 298 K, (b) for 700 K (see also captions of previous figures and text for a detailed discussion).

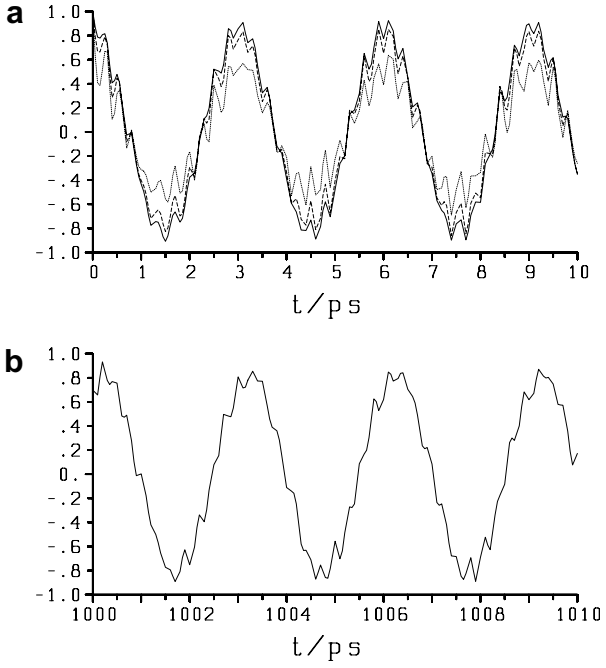

Fig. 12. Chirality χ or enantiomeric excess, Eq. (13), for the wavepackets of Fig. 10 as a function of time (a) initial evolution, full line $T = 298$ K, dashed line $T = 400$ K, dotted line $T = 700$ K (b) long time evolution for 298 K.

τ_R of about 30 fs. One should note that the physical significance of this time is quite different from a high pressure unimolecular relaxation time

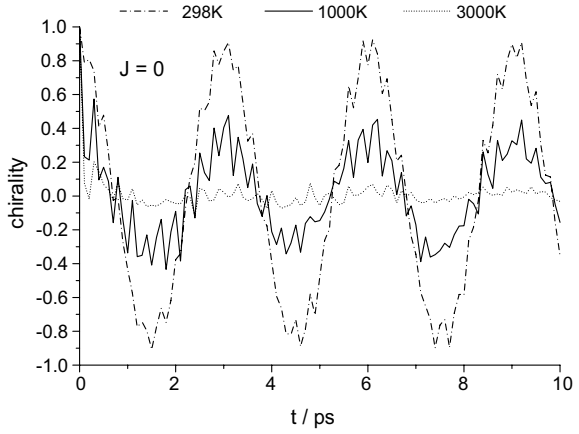

Fig. 13. Evolution of chirality χ as a function of time for quasithermal vibrational–torsional ($J = 0$) wavepackets at 298 K (dashed), 1000 K (full line) and 3000 K (dotted). The sharp peaks result from the limited number of computed timepoints and are thus only a graphical artifact (see also caption to Fig. 12 and text).

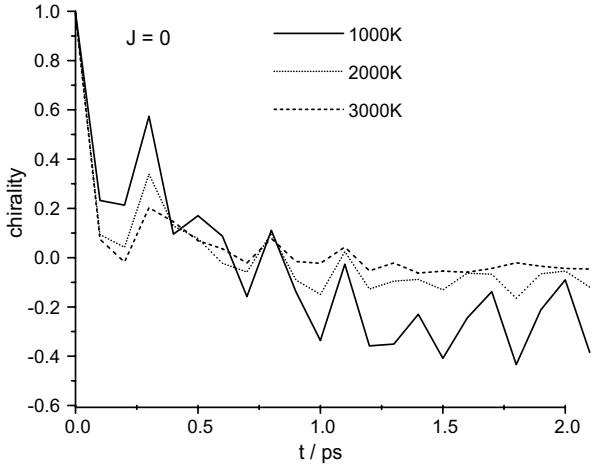

Fig. 14. Detail for short times of Fig. 12 (but $T = 1000$ K, full line, $T = 2000$ K, dotted, and $T = 3000$ K, dashed line).

$$\tau_{R,uni\infty} = \frac{1}{k_{f\infty} + k_{b\infty}} \simeq \frac{1}{2k_{f\infty}}. \tag{15}$$

Rather one has here a randomly sampled collision free ensemble. Nevertheless, if the distributions become comparable then also the relaxation times become comparable. Of course, in order to reach such a collisional high pressure limit relaxation enormous pressures ($p > 10$ kbar) would be needed, which makes the physical situation comparable to the "high pressure limiting relaxation measured at low pressures" and we refer to [98] for a discussion of some of the related fundamental concepts.

We have also calculated approximately the effect of adding rotational motion by approximating the wavefunction roughly as a product of the vibrational wavefunction with a symmetric top wavefunction of appropriate moments of inertia. The rovibrational energies are thus given by $E(v, J, K) = E(v, 0, 0) + (B_z - B_x)K^2 + B_x J(J + 1)$, where

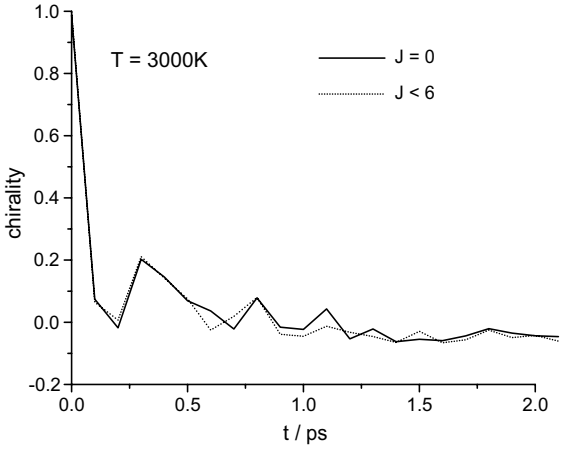

Fig. 15. Chirality calculated from wavepackets at $J = 0$ (3000) and with adding rotational states up to $J < 6$ (see text).

$E(v,0,0)$ are the eigenvalues for the Hamiltonian with $J = 0$, Eq. (2) and B_x and B_z are effective rotational constants. We chose $B_x = 0.85\,\mathrm{cm}^{-1}$ and $B_z = 10.9\,\mathrm{cm}^{-1}$. Fig. 15 shows the resulting slight damping of oscillations with states up to $J < 6$ included. The relaxation time at 3000 K is essentially unaffected. Of course, with explicit full dimensional rotation–vibration coupling the effects may be larger, but such a calculation is still difficult to converge at present.

Fig. 16 finally shows the effect of "smoothing" the probability densities by adding rotational levels. Fig. 16a is a vibrational wavepacket with $J = 0$ randomly sampled at 700 K. Fig. 16b shows the much "smoother" probability densities when including rotational states up to $J < 11$. In agreement with our previous discussions there is very fast transfer of probability from the initial chiral form to its enantiomeric structure within less than 100 fs in both cases, which is much faster than for any of the wavepackets with torsional ground level doublets only. Of course, in the ensembles discussed here, torsional excitation is now included and plays a dominant role. Fig. 17 shows similar results for 298 K, which demonstrates that at this lower temperature the time scales are dominated by low energy tunneling (about 1–2 ps).

One might consider analytical representations for relaxation behaviour in chiral molecules under conditions similar to the ones discussed here. Indeed very simple random relaxation models can be formulated for statistical distributions of tunneling splittings [99]. If a set of splittings D such as those represented in Fig. 4 were to be represented by a rectangular distribution $G(D)$ with constant values for $-D_{\max} \leqslant D \leqslant +D_{\max}$ and $G(D) = 0$ outside this range one finds an oscillatory relaxation for, say $P(M)$

$$P(M) = \frac{1}{2}\left(1 - \frac{\sin(D_{\max}t)}{D_{\max}t}\right). \tag{16}$$

If on the other hand one has a Lorentzian distribution for $G(D)$, say $G_L(D)$, one obtains, indeed an exponential relaxation with

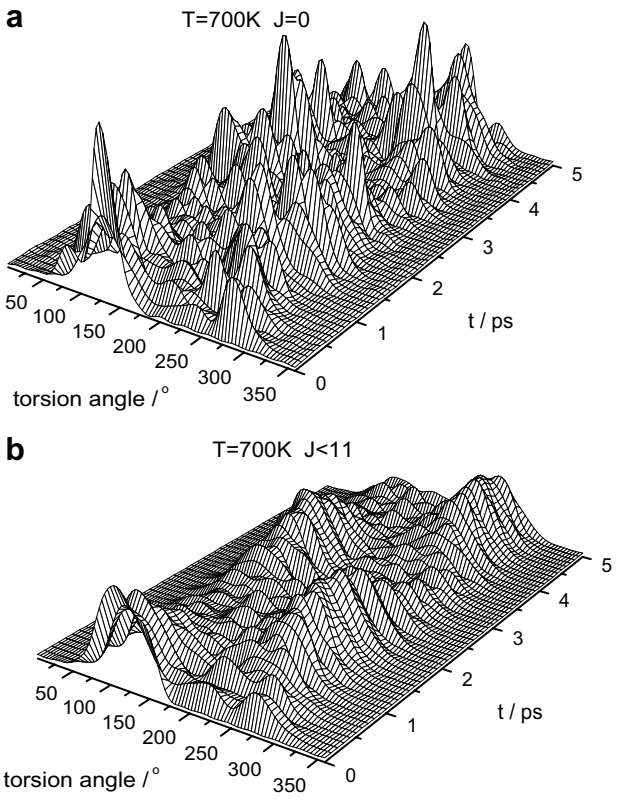

Fig. 16. The effect of adding rotational levels when calculating time dependent probability densities in quasithermal ensembles (a) $T = 700$ K, $J = 0$ (b) $T = 700$ K, with rotational levels up to $J < 11$ (see also captions to Fig. 10 and text).

$$P(M) = \frac{1}{2}[1 - \exp(-D_L t)], \tag{17}$$

where D_L is the half width at half maximum (HWHM) of the Lorentzian distribution.

One might, of course, now proceed to analyse the spectrum of hydrogen peroxide and derive the real distribution function and relaxation behaviour for thermal ensembles of H_2O_2. However, because of the difficulty of an exact treatment of coupling rotation and tunneling-vibration at very high angular momenta, this is still quite difficult. One might also note that much of the reaction at high temperatures proceeds via torsional excitation above the barrier. In fact, one might compare here to a rough transition state estimate for the rate constants and relaxation times and finds without any tunneling (and obvious notations [94,109]):

$$\tau_R = \frac{1}{2k(T)} = \frac{h}{2k_B T}\frac{q}{q^{\neq}}\exp(\Delta E_0/kT). \tag{18}$$

Writing the partition functions of the molecule q and the transition state $q^{\neq}$ in the usual way as a product of functions q_i from the various degrees of freedom and cancelling the partition functions q_i for all degrees of freedom except for torsion with q_T one has thus very simply

$$\tau_R \simeq \frac{h}{2k_B T} q_T \exp(\Delta E_0/kT), \tag{19}$$

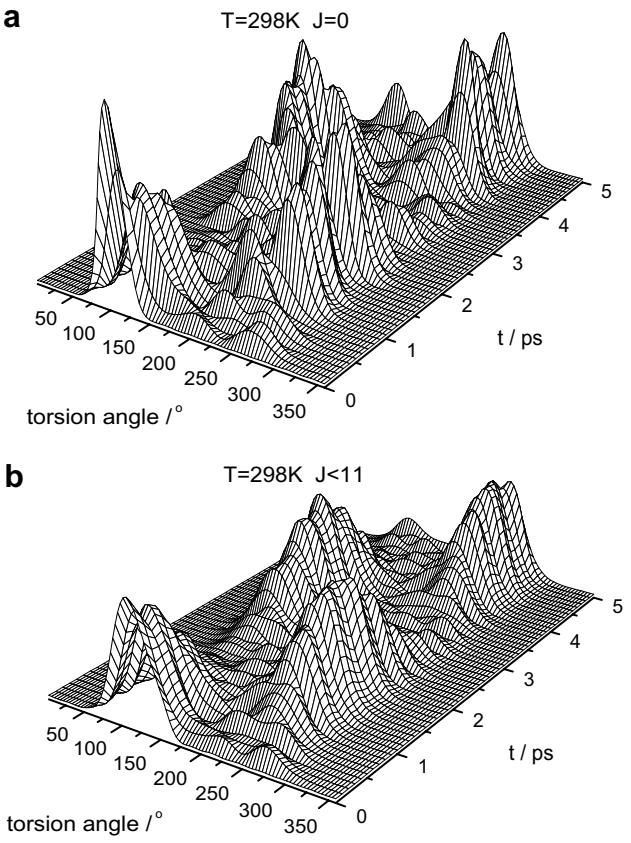

Fig. 17. Probability densities as in Fig. 15, but for 298 K (a) $J = 0$ (b) up to $J < 11$ included.

where ΔE_0 is the effective threshold energy measured from the zero point level. With $\Delta E_0 = 221.5hc\ \mathrm{cm}^{-1}$ from the lowest adiabatic channel and taking the classical limit with $\tilde{\nu}_T = 260\ \mathrm{cm}^{-1}$ this results in about $\tau_R = 90$ fs at 3000 K, which is largely dominated by the torsional frequency and is of the order of magnitude of the result expected from the accurate quantum calculations. Larger deviations are, of course, found at lower temperatures. With the obvious limitations, which such rough estimates have, we see at least that after appreciable averaging and at high temperatures many of the features of the mode selective tunneling quantum dynamics are washed out and the average relaxation times can, indeed, be estimated by the crudest of models.

While this result is not entirely unexpected, we note nevertheless that it relies on the averaging of highly mode specific stereomutation processes and not on fast intramolecular vibrational redistribution, which is unimportant for H_2O_2 under the conditions shown here. Thus the relatively close agreement between the very simple result from transition state theory and the state averaged quantum wavepacket calculations does not demonstrate the validity of the fundamental assumption of intramolecular quasiequilibrium in transition state theory. In fact, as we have shown explicitly here, this assumption is *not* fulfilled. We might mention here the wavepacket calculations on ammonia isotopomer inversion, where IVR plays a more important role [52,53]. Also, one might view our $(5 + 1)$-dimensional quasiadiabatic channel results as a more sophisticated, generalized form of transition state theory [84] and then the agreement between this "quasiadiabatic channel transition state theory" and the exact results would be very good.

4. Conclusions

Hydrogen peroxide stereomutation is among the simplest isomerization reactions, which we have studied here for the isolated molecule by full six-dimensional quantum dynamics on a semiglobal potential energy hypersurface [56], including all vibrational–torsional degrees of freedom. Solutions to the time independent Schrödinger equations provide energy levels and wavefunctions of well defined parity, neglecting the very weak effects from parity violating potentials [67–69,99,100]. This implies that in spite of the chiral nonplanar equilibrium geometry, the energy levels observed by high resolution spectroscopy correspond to effectively achiral states that are describable by superpositions of "left handed" and "right handed" (P and M) enantiomers. The large tunneling splittings of about $\Delta E_{\pm} = 11\ \mathrm{cm}^{-1}$ (hc) compared to the difference of the parity violating potentials of the enantiomers $\Delta_{PV}E \simeq 4 \times 10^{-14}\ \mathrm{cm}^{-1}$ (hc) show that any chiral mixing into the pure parity states would be quite negligible (of the order of $(\Delta E_{\pm}/\Delta_{PV}E)^{-2}$). This situation is anticipated for molecules with tunneling in the "low barrier limit" and is quite common in the spectroscopy of such molecules. The levels can be grouped, however, in pairs of levels of different parity separated by a splitting that is small compared with the vibrational fundamental spacings. The splitting can be associated with the stereomutation time for appropriate chiral superposition states. This shows a high degree of mode selectivity [57,64–66,78] when exciting different vibrational fundamentals and generates an interesting systematic behaviour for various combination and overtone levels, in spite of superficially "random" overall appearance. We have discussed that a more proper understanding of the real stereomutation dynamics requires a detailed investigation of the time dependent wavefunctions with an initially chiral state. In relation to the questions addressed in the introduction, our investigation along these lines has provided the following main conclusions.

1. The multidimensional wavepackets, indeed, confirm the high degree of mode selectivity in catalyzing or inhibiting stereomutation when exciting various vibrational modes other than torsion. The antisymmetric O–O–H bending mode ν_6 is a strongly catalyzing mode, whereas the symmetric bending mode ν_2 and the stretching modes ν_1 and ν_5 are inhibiting modes. The O–O stretching mode ν_3 is an almost inactive spectator mode. The wavepacket results shown here in an exemplary manner for the mode ν_6 confirm what would have been inferred

from the various previous eigenstate analyses. This might have been expected, but is not a priori guaranteed. This behaviour is related to the results discussed in the following conclusions.

2. The nature of the wavepacket motion at energies high above the *trans*-barrier for stereomutation (only about 360 cm^{-1}, less than all the vibrational fundamentals except torsion) is governed by quasiadiabatic above barrier tunneling. The wavepacket behaviour is qualitatively similar to the ground state wavepacket below the barrier, only its period of motion is changed. The periodic stereomutation process is essentially maintained for long times of at least 100 ps. Quasiadiabatic above barrier tunneling complements the first discussion of the tunnel effect of chiral molecules in the ground state as discovered by Hund 8 decades ago [110].
3. The quasiadiabatic channel RPH approximation is very successful in describing both the energy level spectrum and eigenfunctions as well as the time dependent wavepacket motion in the ground state and in the quasiadiabatic above barrier tunneling discussed above. Differences to the exact results remain small up to energies of 4000 cm^{-1}, where exact calculations are available. Approximate results for very high OH stretching polyads seem to indicate effectively quasiadiabatic above barrier tunneling up to energies near the lowest dissociation limit corresponding to the $N = 5$ and $N = 6$ polyads (15,000–20,000 cm^{-1}) with a consistently and strongly decreasing tunneling rate with increasing OH stretching excitation. This result is of interest in principle, by showing the possibility of using the inverse superposition scheme with tunneling switching to study parity violation in molecules of the general type similar to H_2O_2 [63,99,101,102], although H_2O_2 itself is clearly unsuitable for such experiments because of the much too large tunneling splittings at all energies.
4. Choosing initial conditions of localized chiral wavepackets drawn from a random quasithermal ensemble one finds an increasing tendency towards relaxation-like behaviour, which can be qualitatively understood by simple models and may show either oscillatory or exponential relaxation. Such relaxation and racemisation for stereomutation in the low barrier limit can be compared to femtosecond wavepacket racemisation by intramolecular vibrational redistribution (IVR) in molecules that are achiral at the equilibrium geometry but may have an initial wavepacket state that is chiral [103,111,112]. One can also compare to coupled IVR and tunneling in ammonia [51,52]. The relaxation times of the quasithermal wavepackets at high temperatures are only weakly temperature dependent on the order of 30 fs at 1000–3000 K. One can compare these times with transition state approximations that are used in reaction dynamics. The quasiadiabatic channel RPH approximation can be considered to be a generalized transition state model with tunneling and as it describes even the mode selective wavepacket results accurately, it will also describe the torsional relaxation rates with similar accuracy. However, the most commonly used quasiharmonic transition state theory without tunneling, using harmonic frequencies for the equilibrium geometries and transition state geometries to calculate partition functions, will give reasonable results only at high temperatures (3000 K with kT exceeding the barrier by more than a factor of 5) and fails at low temperature. Anharmonic corrections (without tunneling) will not change this conclusion. A similar conclusion can be drawn by inference for classical trajectory results: While they may be adequate for thermal rates at high temperatures, they will fail for low temperatures. While such a conclusion might have been anticipated by some, it is certainly not widely appreciated in applications to similar reaction systems. Interestingly, the acceptable validity at high temperatures arises here from averaging, not from fast mode–mode coupling (IVR). While we have also studied approximately the role of rotation, accurate results on this will have to be derived in future work.

We can also draw some conclusions of a more general nature. The time dependent wavefunctions and probability densities discussed in the present work can be translated into other time dependent chiral observables such as optical activity, circular dichroism or Raman optical activity. By this, we can relate our results also to more ordinary kinetic experiments, where, indeed, time dependent optical activity was the first observable studied in quantitative kinetic experiments [6,104] and might be conceptually related today to the possible femtosecond observation of optical activity in reactions of chiral molecules. Indeed, there has been much recent interest in "direct" time dependent observation of tunneling processes on very short time scales [105,106] (see also [107]). We would claim that our results provide the basis for a "high resolution spectroscopic" approach to short time stereomutation tunneling dynamics in H_2O_2. This is true to the extent that the Hamiltonian is spectroscopically adjusted [108]. The time resolution that one can claim for such an approach is $\Delta t > 1/(4\pi c \Delta\tilde{\nu})$. If we take the limit of accurate analysis in the present work on H_2O_2 to be about 5000 cm^{-1}, then this corresponds to a time resolution for general vibrational–torsional-tunneling dynamics of $\Delta t > 530$ attoseconds (as). Approximate extension of the analysis to 20,000 cm^{-1} leads to $\Delta t > 130$ as, which is comparable to the best "direct" time resolved results.

Acknowledgements

Help from, discussion and correspondence with Z. Guennoun, Hans Hollenstein, B. Kuhn, R. Marquardt, T. Rizzo, J. Stohner, M. Suhm and M. Willeke are gratefully acknowledged. Our work is supported financially by ETH Zurich (including AGS, C^4 and CSCS) and the Schweizerischer Nationalfonds.

References

[1] (a) E. Schrödinger, Naturwissenschaften 14 (1926) 664;
(b) E. Schrödinger, Ann. d. Physik, 4. Folge, Bd. 81 (1926) 109.
[2] M. Bixon, J. Jortner, J. Chem. Phys. 48 (1968) 715.
[3] J. Jortner, S.A. Rice, R.M. Hochstrasser, Adv. Photochem. 7 (1969) 149.
[4] R.D. Levine, Quantum Mechanics of Molecular Rate Processes, Clarendon Press, Oxford, 1969.
[5] J. Manz, in: V. Sundström (Ed.), Femtochemistry and Femtobiology: Ultrafast Reaction Dynamics at Atomic-Scale Resolution, Nobel Symposium 101, Björkborn, Sweden, September 9–12, 1996, vol. 3, Imperial College Press, London, 1997, p. 80.
[6] M. Quack, Chimia 55 (2001) 753.
[7] R.V. Ambartzumian, Y.A. Gorokhov, V.S. Letokhov, G.N. Makarov, JETP Lett. 21 (1975) 171.
[8] J.L. Lyman, R.J. Jensen, J. Rink, C.P. Robinson, S.D. Rockwood, Appl. Phys. Lett. 27 (1975) 87.
[9] E.R. Grant, P.A. Schulz, A.S. Sudbo, Y.R. Shen, Y.T. Lee, Phys. Rev. Lett. 40 (1978) 115.
[10] M. Quack, J. Chem. Phys. 69 (1978) 1282.
[11] M. Quack, in: K. Lawley, I. Prigogine, S.A. Rice (Eds.), Adv. Chem. Phys, vol. 50, John Wiley, New York, USA, 1982, p. 395.
[12] M. Quack, Infrared Phys. 29 (1989) 441.
[13] M. Quack, in: P. von Ragué Schleyer, N. Allinger, T. Clark, J. Gasteiger, P.A. Kollman, H.F. Schaefer, P.R. Schreiner (Eds.), Encyclopedia of Computational Chemistry, vol. 3, Wiley, New York, 1998, p. 1775.
[14] J. Manz, L. Wöste (Eds.), Femtosecond Chemistry, Proc. Berlin Conf. Femtosecond Chemistry (Berlin, March 1993), Verlag Chemie, Weinheim, 1995.
[15] J. Manz, A.W. Castleman, J. Phys. Chem. 97 (1993) 12423.
[16] D.W. Lupo, M. Quack, Chem. Rev. 87 (1987) 181.
[17] M. Quack, Ber. Bunsenges. Phys. Chem. 83 (1979) 1287.
[18] M. Shapiro, P. Brumer, Principles of the Quantum Control of Molecular Processes, Wiley–Interscience, Hoboken, 2003.
[19] R.S. Judson, H. Rabitz, Phys. Rev. Lett. 68 (1992) 1500.
[20] D.J. Tannor, S.A. Rice, Adv. Chem. Phys. 70 (1988) 441.
[21] C. Daniel, J. Full, L. Gonzalez, C. Lupulescu, J. Manz, A. Merli, S. Vajda, L. Wöste, Science 299 (2003) 536.
[22] Y. Fujimura, L. Gonzalez, K. Hoki, D. Kroner, J. Manz, Y. Ohtsuki, Angew. Chem. Int. Ed. 39 (2000) 4586.
[23] R. Marquardt, M. Quack, Z. Phys. D 36 (1996) 229.
[24] C. Hiller, J. Manz, W.H. Miller, J. Romelt, J. Chem. Phys. 78 (1983) 3850.
[25] B. Hartke, J. Manz, J. Mathis, Chem. Phys. 139 (1989) 123.
[26] J. Manz, C.S. Parmenter, Chem. Phys. 139 (1989) U1.
[27] M. Quack, E. Sutcliffe, Chem. Phys. Lett. 105 (1984) 147.
[28] F.F. Crim, J. Phys. Chem. 100 (1996) 12725.
[29] F. Fernández-Alonso, B.D. Bean, J.D. Ayers, A.E. Pomerantz, R.N. Zare, L. Banares, F.J. Aoiz, Angew. Chem. Int. Ed. 39 (2000) 2748.
[30] R.N. Zare, Science 311 (2006) 1383.
[31] J.P. Camden, H.A. Bechtel, D.J.A. Brown, R.N. Zare, J. Chem. Phys. 124 (2006). Art. No. 034311.
[32] T.R. Rizzo, Chimia 50 (1996) 581.
[33] A. Callegari, T.R. Rizzo, Chem. Soc. Rev. 30 (2001) 214.
[34] R. Marquardt, M. Quack, J. Stohner, E. Sutcliffe, J. Chem. Soc., Faraday Trans. 2 82 (1986) 1173.
[35] R. Marquardt, M. Quack, J. Chem. Phys. 95 (1991) 4854.
[36] M.J. Rosker, T.S. Rose, A.H. Zewail, Chem. Phys. Lett. 146 (1988) 175.
[37] A.H. Zewail, Science 242 (1988) 1645.
[38] G. Porter, in: J. Manz, L. Woeste (Eds.), Femtosecond Chemistry, vol. 1, Verlag Chemie, Weinheim, 1995, p. 3.
[39] A.H. Zewail, in: J. Manz, L. Woeste (Eds.), Femtosecond Chemistry, vol. 2, Verlag Chemie, Weinheim, 1995, p. 15.
[40] G.R. Fleming, Chemical Applications of Ultrafast Spectroscopy, Oxford University Press, Oxford, 1986.
[41] A.H. Zewail, Angew. Chem. Int. Ed. 39 (2000) 2587.
[42] W.F. van Gunsteren, H.J.C. Berendsen, Angew. Chem. Int. Ed. Engl. 29 (1990) 992.
[43] R. Car, M. Parrinello, Phys. Rev. Lett. 55 (1985) 2471.
[44] W.H. Miller, J. Chem. Phys. 125 (2006) 132305.
[45] F. Mariotti, M. Quack, M. Willeke, J. Stohner, Chimia 58 (2004) 263.
[46] K. von Puttkamer, M. Quack, Chem. Phys. 139 (1989) 31.
[47] M. Quack, M.A. Suhm, Mol. Phys. 69 (1990) 791.
[48] M. Quack, M.A. Suhm, Chem. Phys. Lett. 234 (1995) 71.
[49] W. Klopper, M. Quack, M.A. Suhm, Chem. Phys. Lett. 261 (1996) 35.
[50] W. Klopper, M. Quack, M.A. Suhm, J. Chem. Phys. 108 (1998) 10096.
[51] R. Marquardt, M. Quack, I. Thanopulos, D. Luckhaus, J. Chem. Phys. 118 (2003) 643.
[52] R. Marquardt, M. Quack, I. Thanopulos, D. Luckhaus, J. Chem. Phys. 119 (2003) 10724.
[53] R. Marquardt, K. Sagui, W. Klopper, M. Quack, J. Phys. Chem. B 109 (2005) 8439.
[54] M. Snels, H. Hollenstein, M. Quack, J. Chem. Phys. 119 (2003) 7893.
[55] M. Snels, H. Hollenstein, M. Quack, J. Chem. Phys. 125 (2006) 194319.
[56] B. Kuhn, T.R. Rizzo, D. Luckhaus, M. Quack, M.A. Suhm, J. Chem. Phys. 111 (1999) 2565.
[57] B. Fehrensen, D. Luckhaus, M. Quack, Chem. Phys. Lett. 300 (1999) 312.
[58] R. Berger, M. Gottselig, M. Quack, M. Willeke, Angew. Chem. Int. Ed. 40 (2001) 4195.
[59] M. Quack, M. Willeke, Helv. Chim. Acta 86 (2003) 1641.
[60] M. Gottselig, D. Luckhaus, M. Quack, J. Stohner, M. Willeke, Helv. Chim. Acta 84 (2001) 1846.
[61] M. Gottselig, M. Quack, M. Willeke, Isr. J. Chem. 43 (2003) 353.
[62] M. Gottselig, M. Quack, J. Stohner, M. Willeke, Int. J. Mass Spectrom. 233 (2004) 373.
[63] M. Quack, M. Willeke, J. Phys. Chem. A 110 (2006) 3338.
[64] D. Luckhaus, J. Chem. Phys. 113 (2000) 1329.
[65] R.Q. Chen, G.B. Ma, H. Guo, J. Chem. Phys. 114 (2001) 4763.
[66] R.Q. Chen, G.B. Ma, H. Guo, Chem. Phys. Lett. 320 (2000) 567.
[67] A. Bakasov, T.K. Ha, M. Quack, J. Chem. Phys. 109 (1998) 7263.
[68] R. Berger, M. Quack, J. Chem. Phys. 112 (2000) 3148.
[69] A. Bakasov, R. Berger, T.K. Ha, M. Quack, Int. J. Quantum Chem. 99 (2004) 393.
[70] R. Berger, N. Langermann, C. van Wüllen, Phys. Rev. A 71 (2005) 042105.
[71] R. Berger, C. van Wüllen, J. Chem. Phys. 122 (2005) 134316.
[72] M. Quack, J. Stohner, Chimia 59 (2005) 712.
[73] M. Quack, in: K.J. Naidoo, J. Brady, M.J. Field, J. Gao, M. Hann (Eds.), Modelling Molecular Structure and Reactivity in Biological Systems, Proc. 7th WATOC Congress, Cape Town January 2005, Royal Society of Chemistry, Cambridge, 2006, p. 3.
[74] B. Fehrensen, D. Luckhaus, M. Quack, Z. Phys. Chem. 209 (1999) 1.
[75] J. Koput, S. Carter, N.C. Handy, J. Phys. Chem. A 102 (1998) 6325.
[76] J. Koput, S. Carter, N.C. Handy, J. Chem. Phys. 115 (2001) 8345.
[77] D. Luckhaus, M. Quack, Chem. Phys. Lett. 190 (1992) 581.
[78] V.A. Benderskii, I.S. Irgibaeva, E.V. Vetoshkin, H.P. Trommsdorff, Chem. Phys. 262 (2000) 369.
[79] W.H. Miller, N.C. Handy, J.E. Adams, J. Chem. Phys. 72 (1980) 99.
[80] L. Hofacker, Z. Naturforsch. A 18 (1963) 607.
[81] R.A. Marcus, J. Chem. Phys. 43 (1965) 1598.
[82] J.T. Hougen, P.R. Bunker, J.W.C. Johns, J. Mol. Spectrosc. 34 (1970) 136.
[83] M. Quack, J. Troe, Ber. Bunsenges. Phys. Chem. 78 (1974) 240.

[84] M. Quack, J. Troe, in: P. von Ragué Schleyer, N. Allinger, T. Clark, J. Gasteiger, P.A. Kollman, H.F.I. Schaefer, P.R. Schreiner (Eds.), Encyclopedia of Computational Chemistry, vol. 4, Wiley, 1998, p. 2708.
[85] M. Quack, M.A. Suhm, J. Chem. Phys. 95 (1991) 28.
[86] M. Quack, M.A. Suhm, Chem. Phys. Lett. 183 (1991) 187.
[87] M. Quack, J. Phys. Chem. 83 (1979) 150.
[88] W.B. Olson, R.H. Hunt, B.W. Young, A.G. Maki, J.W. Brault, J. Mol. Spectrosc. 127 (1988) 12.
[89] A. Perrin, A. Valentin, J.M. Flaud, C. Camy-Peyret, L. Schriver, A. Schriver, P. Arcas, J. Mol. Spectrosc 171 (1995) 358.
[90] C. Camy-Peyret, J.M. Flaud, J.W.C. Johns, M. Noel, J. Mol. Spectrosc. 155 (1992) 84.
[91] W.B. Cook, R.H. Hunt, W.N. Shelton, F.A. Flaherty, J. Mol. Spectrosc. 171 (1995) 91.
[92] P. Helminger, W.C. Bowman, F.C. De Lucia, J. Mol. Spectrosc. 85 (1981) 120.
[93] L.B. Harding, J. Phys. Chem. 93 (1989) 8004.
[94] E.R. Cohen, T. Cvitas, J.G. Frey, B. Holmström, K. Kuchitsu, R. Marquardt, I. Mills, F. Pavese, M. Quack, J. Stohner, H.L. Strauss, M. Takami, A.J. Thor, Quantities, Units and Symbols in Physical Chemistry, third ed., IUPAC, RSC Publishing, Cambridge, 2007.
[95] B. Fehrensen, M. Hippler, M. Quack, Chem. Phys. Lett. 298 (1998) 320.
[96] R. Marquardt, M. Quack, J. Phys. Chem. 98 (1994) 3486.
[97] M. Quack, E. Sutcliffe, Infrared Phys. 25 (1985) 163.
[98] M. Quack, Ber. Bunsenges. Phys. Chem. 88 (1984) 94.
[99] M. Quack, Angew. Chem. Int. Ed. 28 (1989) 571.
[100] A. Bakasov, M. Quack, Chem. Phys. Lett. 303 (1999) 547.
[101] M. Quack, Chem. Phys. Lett. 132 (1986) 147.
[102] M. Quack, Faraday Discuss. 99 (1994) 390.
[103] R. Marquardt, M. Quack, I. Thanopulos, J. Phys. Chem. A 104 (2000) 6129.
[104] L. Wilhelmy, Ann. Phys. 81 (1850) 413.
[105] J.P. Marangos, Nature 446 (2007) 619.
[106] M. Uiberacker, T. Uphues, M. Schultze, A.J. Verhoef, V. Yakovlev, M.F. Kling, J. Rauschenberger, N.M. Kabachnik, H. Schroder, M. Lezius, K.L. Kompa, H.G. Muller, M.J.J. Vrakking, S. Hendel, U. Kleineberg, U. Heinzmann, M. Drescher, F. Krausz, Nature 446 (2007) 627.
[107] H. Niikura, F. Legare, D.M. Villeneuve, P.B. Corkum, J. Mod. Opt. 52 (2005) 453.
[108] M. Quack, Molecular femtosecond quantum dynamics between less than yoctoseconds and more than days: experiment and theory, in: J. Manz, L. Woeste (Eds.), Femtosecond Chemistry, Proc. Berlin Conf. Femtosecond Chemistry, Berlin (March 1993), Verlag Chemie, Weinheim, 1995, p. 781 (Chapter 27).
[109] D. Luckhaus, M. Quack, in: J.H. Moore, N. Spencer (Eds.), Encyclopedia of Chemical Physics and Physical Chemistry, vol. 1, IOP Publishing, Bristol, 2001, p. 653 (Chapter A3.4).
[110] (a) F. Hund, Z. Physik. 40 (1926) 742;
(b) F. Hund, Z. Physik. 42 (1927) 805.
[111] R. Marquardt, M. Quack, in: J.H. Moore, N. Spencer (Eds.), Encyclopedia of Chemical Physics and Physical Chemistry, vol. 1, IOP Publishing, Bristol, 2001, p. 897 (Chapter A3.13).
[112] D. Luckhaus, M. Quack, in: J.H. Moore, N. Spencer (Eds.), Encyclopedia of Chemical Physics and Physical Chemistry, vol. 2, IOP Publishing, Bristol, 2001, p. 1871 (Chapter B2.5).